Malaysian Journal of Energy and Applications 1 (2026): 1-23
https://doi.org/10.17576/myjea.2026.01.1

QUANTIFYING SYNERGISTIC ENERGY LOSSES INDUCED BY INTERNAL RESISTANCE IN MICROBIAL FUEL CELL BIOANODES: THE ROLE OF PHYSICAL CONNECTIVITY AND IONIC STRENGTH

Nor Syazwanie Mohd Saidi, Muhammad Farhan Hil Me, Yashawini Phriya Rauichandran, Ryan Yow Zhong Yeo, Mohammad Sherjeel Javed Khan, Swee Su Lim*

Fuel Cell Institute (SELFUEL), Universiti Kebangsaan Malaysia, 43600 UKM Bangi, Selangor, Malaysia

**Corresponding author: limss@ukm.edu.my*

Received 4/4/2026; Received in Revised Form 13/6/2026; Accepted 13/6/2026; Available Online 20/07/2026.

Abstract

Internal resistance R_{int} is a critical bottleneck that dictates the power output and efficiency of microbial fuel cells (MFCs). This study investigates the synergistic impact of gradated internal resistance on bioanode performance by systematically manipulating electrode contact integrity to establish three distinct R_{int} levels: 20 Ω (Group 1), 60 Ω (Group 2), and 182 Ω (Group 3). Results indicate that elevated R_{int} triggers a cascade of potential energy losses; Group 3 exhibited a 22% reduction in peak power density (0.07 W/m^2) compared to the optimized Group 1 (0.09 W/m^2). Electrochemical Impedance Spectroscopy (EIS) identified the anodic interface as the primary site of degradation, with interfacial resistance (R_2) surging from 3 Ω in Group 1 to 140.19 Ω in Group 3. Cyclic Voltammetry (CV) revealed that high R_{int} might have altered the redox behavior in the electrogenic biofilm, evidenced by a +0.36 V positive transition in midpoint potential (E_{mid}), suggesting increased electrochemical energy demand and altered apparent redox behavior. Furthermore, sensitivity analysis via One-Factor-at-a-Time (OFAT) optimization identified a 10:5:50 mM (NaAc:NH4Cl:PBS) electrolyte ratio as optimal, driving current density to a peak of ≈ 2.1 A/m^2 by mitigating secondary chemical bottlenecks. These findings suggest that poor connection is not merely a hardware failure but an electrochemical stress factor that affects the catalytic response of the bioelectrochemical interface.

Keywords: Bioanode kinetics, internal resistance gradation, electrochemical impedance spectroscopy (EIS), charge transfer resistance, microbial electron transfer pathways.

Introduction

The escalating trajectory of global energy consumption and the concomitant surge in wastewater contamination represent two of the most formidable challenges of the 21st century. As of 2026, global energy demand continues to rise, driven by industrialization and population growth, while "water bankruptcy"—the state where water demand exceeds sustainable supply—afflicts nearly one-third of the world's population (Wang et al., 2026). Environmental pollution has reached critical levels, with untreated industrial and domestic effluents severely degrading aquatic ecosystems worldwide (Boutarbouch et al., 2026; Kurniawan et al., 2026). These challenges directly impede the progress of the United Nations Sustainable Development

Goals (SDGs), specifically SDG 6 (Clean Water and Sanitation) and SDG 7 (Affordable and Clean Energy), which mandate a global shift toward sustainable resource recovery (Baba et al., 2026; Saghir et al., 2026). Locally, this claim is strengthened by the National Energy Policy (DTN) 2022–2040 and the Water Sector Transformation 2040 (WST 2040), which emphasize Malaysia's commitment to achieving a low-carbon economy and a circular water cycle through the adoption of indigenous, high-efficiency green technologies (Rani et al., 2025).

Traditional wastewater management relies heavily on conventional biological treatments, such as activated sludge processes. While effective, these methods are characterized by massive energy footprints, primarily due to the aeration required to oxidize organic and inorganic contaminants to meet standard discharge values for Chemical Oxygen Demand (COD) and Biochemical Oxygen Demand (BOD) (Ravindran et al., 2025). Globally, discharge standards are becoming increasingly stringent; for instance, many international frameworks now mandate BOD levels below 10–20 mg/L before environmental release. Locally, the Department of Environment (DOE) Malaysia enforces the Environmental Quality (Industrial Effluents) Regulations, which categorize discharge into Standard A (for upstream catchments) and Standard B (for downstream areas), necessitating advanced treatment to reach these benchmarks (*Environmental Requirements: A Guide For Investors* 2010).

Beyond biological methods, alternative treatments such as advanced electrochemical oxidation (EO), adsorption, and chemical precipitation are frequently employed to meet stringent discharge standards, such as Standard A and B enforced by the Department of Environment (DOE) Malaysia. Advanced electrochemical oxidation (EO) utilizes electrical energy to generate highly reactive hydroxyl radicals (·OH) at an anode to mineralize complex pollutants, such as textile dyes or landfill leachate, into CO_2 and water (Solomon et al., 2020; Wilk et al., 2022). In contrast, adsorption is a surface-based phenomenon where molecules adhere to solids like activated carbon or biochar to remove pharmaceutical residues or heavy metals, while chemical precipitation utilizes reagents like lime or alum to turn dissolved contaminants into insoluble solids for sedimentation (Nemeș et al., 2026). Although effective, these technologies incur high operational costs due to significant electrical energy inputs and the continuous requirement for chemical reagents, highlighting the need for passive, energy-recovering alternatives like Microbial Fuel Cells (MFCs) (Feng et al., 2024).

Microbial Fuel Cells (MFCs) have emerged as a transformative technology capable of simultaneous wastewater treatment and bioelectricity generation. The core principle involves the use of electrochemically active microorganisms to catalyze the oxidation of organic matter in wastewater, converting chemical energy directly into electrical energy (Feng et al., 2024; Musa et al., 2026). A typical microbial fuel cell (MFC) functions through the coordinated action of several essential components: an anode where anaerobic microbes oxidize substrates like acetate to release electrons and protons, a cathode where these electrons arriving via an external circuit combine with protons and an oxygen electron acceptor to form water, and a membrane (such as a Cation Exchange Membrane) that facilitates proton transport while preventing oxygen crossover. Central to this process is the microbial consortium, often enriched from sludge or existing electrochemical systems to establish an electrogenic biofilm that serves as the metabolic engine of the device (Lim et al., 2021; Nawaz et al., 2020; Zadeh et al., 2024).

Despite their potential, the practical application of MFCs is hindered by significant technical bottlenecks that limit power density and scalability (Mahmoud et al., 2022). Literature suggests various strategies for improvement, including electrode modification and optimizing microbial communities (Hegazy et al., 2025; Zadeh et al., 2024). However, a fundamental limiting factor that requires deeper mechanistic understanding is internal

resistance. Internal resistance (R_{int}) plays a pivotal role in the operational efficiency of bioelectrochemical systems (BES), serving as a primary determinant of the manageable power output. In systems such as MFCs, R_{int} is comprised of ohmic, activation, and mass-transport overpotentials which collectively dictate the rate of extracellular electron transfer (EET) (Kanani et al., 2025). As this resistance increases, it significantly impedes the flow of electrons from the electrogenic biofilm to the electrode surface, resulting in a substantial decrease in the overall electrochemical performance of the BES. Consequently, a fundamental objective in BES engineering is to maintain R_{int} at the lowest possible threshold to eliminate potential energy losses and maximize thermodynamic efficiency (Kim et al., 2021).

While many studies focus on the chemical aspects of resistance, such as ionic strength and substrate availability, the impact of physical connectivity—specifically the contact integrity between the electrode and current collector—is often overlooked. Poor physical connections are not merely passive resistors; they may alter the electrochemical environment of the bioanode. To investigate this critical role, three distinct levels of internal resistance were systematically established in this study (20, 60, and 182 **Ω**) to map the mechanistic insights into electricity generation at the bioanode. The performance of these systems was evaluated by recording and analyzing power and current generation profiles. To provide a high-resolution breakdown of the kinetic bottlenecks, advanced electrochemical characterizations including cyclic voltammetry (CV) and electrochemical impedance spectroscopy (EIS) were utilized. Specifically, these tools allow for the partitioning of charge transfer and interfacial resistances, facilitating a deeper understanding of how physical poor connections escalate activation and mass transport limitation. This study aims to clarify whether bioanode performance degradation is a matter of perception or a direct consequence of poor physical connection integrity.

Unlike previous MFC studies that mainly examined internal resistance through electrode spacing, membrane type, electrolyte conductivity, substrate concentration, or reactor architecture, this study specifically isolates poor physical contact between the electrode and current collector as a controlled source of internal resistance. By creating three resistance levels and combining polarization, EIS, and CV analysis, this work provides a diagnostic framework for identifying how physical connection quality contributes to ohmic, interfacial, activation, and apparent mass-transport losses in MFC bioanodes.

Materials and Methods

Reactor Configuration and Bioanode Enrichment

The experimental architecture, including the schematic of the microbial fuel cell (MFC) and the laboratory-scale assembly, is detailed in Figure 1. Six identical dual-chamber bioelectrochemical systems (BES) were operated as MFCs. Each reactor was constructed from two symmetrical polyacrylic blocks with external dimensions of 70 × 70 × 20 mm (See Figure 1(c)). The internal compartments were precision-fabricated to 50 × 50 × 10 mm, providing a net working volume of 25 mL per chamber. The reactor assembly was secured using four M5 diagonal screws to ensure a leak-proof seal. The electrode assembly and membrane specifications were as follows:

- **Anode:** Plain carbon felt (5 ×5 ×1 cm) served as the bioanode.
- **Cathode:** Carbon felt of identical dimensions, coated with 0.5 mg Pt/cm^2 to facilitate the oxygen reduction reaction (ORR).

- **Membrane:** A cation exchange membrane (CMI-7000, Membrane International Inc.) was positioned between the chambers to mediate proton transport.

Saturated silver-silver chloride (Ag/AgCl) reference electrodes (REs) were utilized to provide a stable potential baseline for all measurements. As illustrated in Figure 1(b), the REs were positioned at a fixed distance of approximately 0.5 cm from the respective working electrodes (anode and cathode) to minimize iR drop during data acquisition. A conversion factor of +0.197 vs. Ag/AgCl was applied to align the data with the Standard Hydrogen Electrodes (SHE) scale at 25°C unless stated otherwise.

Controlled Internal Resistance Gradation

To investigate the critical role of internal resistance and provide mechanistic insights into the resulting bioelectrochemical behavior, a controlled resistance gradient was established across the test groups. The contact integrity between the carbon felt electrodes and the titanium wire connectors (facilitating the external circuit interface) was systematically manipulated to simulate varying degrees of connection quality. These modifications were designed to create three distinct levels of internal resistance (R_{int}) as categorized in Table 1.

Table 1 Experimental Design and Controlled Internal Resistance (R_{int}) Gradation

MFC Group	Connection Integrity	Targeted R_{int} (Ω)	Resistance Multiplier	Research Objective
1	Optimized, high-integrity contact	**20**	1× (Baseline)	Establish baseline bioelectrochemical performance.
2	Moderate manual loosening of Ti-electrode interface	**60**	3×	Study intermediate potential energy losses and kinetic shifts.
3	Significant contact restriction / poor connectivity	**180**	9×	Simulate severe connection gaps and synergistic energy losses.

The internal resistance levels were created by adjusting the physical contact between the carbon felt electrode and the titanium wire current collector. The titanium wire was tied to the carbon felt to provide the electrical connection between the electrode and the external circuit. For the optimized connection condition, the titanium wire was tied firmly to ensure good contact with the carbon felt. For the higher-resistance conditions, the titanium wire was gradually loosened to reduce the contact between the titanium wire and carbon felt. The degree of loosening was adjusted until the desired internal resistance levels were obtained.

The internal resistance was estimated from the voltage response of the MFC under no-load and under-load conditions. The open-circuit voltage was first measured using a digital multimeter under no-load condition. The circuit was then connected to a known external resistance, and the loaded voltage was measured. The internal resistance was calculated by comparing the no-load voltage and loaded voltage with the known external resistance. The reported resistance values of 20, 60, and 182 Ω represent calculated values obtained from these voltage measurements. The measurements were performed before and after the experiment to confirm that the resistance levels remained consistent throughout the operation. This procedure was carried out to ensure that the observed performance differences were mainly related to the controlled physical connection condition rather than uncontrolled changes in the electrode assembly.

All configurations were operated in duplicate to assess reproducibility. This deliberate gradation allowed for the precise mapping of how physical connection gaps—often perceived as minor assembly errors—affect the activation, ohmic, and apparent mass-transport kinetics of the bioanode.

Inoculation and Media Composition

The microbial inoculum was sourced from a combination of sediment collected from the UKM Engineering Lake and an existing microbial fuel cell (MFC) setup that had been in continuous operation for over three years. The inoculation process involved mixing the concentrated sludge with the anodic medium at a 1:1 ratio. The chemical compositions of the electrolytes were:

- **Anolyte:** Sodium acetate (0.41 g/L) as the primary electron donor, supplemented with NH_4Cl (1.07 g/L), KCl (0.11 g/L), $NaH_2PO_4 \cdot 2H_2O$ (0.66 g/L), $Na_2HPO_4 \cdot 2H_2O$ (1.03 g/L), and Wolfe's mineral/vitamin solutions. The basal medium was autoclaved at 121°C for 20 minutes. Post-sterilization, the Wolfe's mineral and vitamin solutions were added via 0.2 µm membrane filtration to prevent thermal degradation. To ensure anaerobic conditions, the completed medium was purged with high-purity nitrogen (N_2) to remove dissolved oxygen prior to use.
- **Catholyte:** A 50 mM phosphate buffer (pH 7.0) comprising $NaH_2PO_4 \cdot 2H_2O$ (3.30 g/L), $Na_2HPO_4 \cdot 2H_2O$ (5.14 g/L), and KCl (0.11 g/L). The catholyte was air-saturated via an aquarium pump to maintain dissolved oxygen (DO) levels above 3 mg/L.

Operational Start-up and Data Acquisition

The complete experimental configuration was assembled as illustrated in Figure 1(a). The anolyte and catholyte were fed independently from 5 L reservoirs into their respective chambers at a constant flow rate of 0.17 mL/min using a multi-channel peristaltic pump. The operational protocol was executed in the following stages:

- **Inoculation:** The inoculum source was injected into the anodic chambers, and the remaining volume was filled with the stock medium.
- **Monitoring:** Potential was monitored via a data logger (Pico ADC-16) and PicoLog software, with data points recorded at 15-minute intervals.
- **Conditioning:** The reactors were initially maintained under open-circuit conditions for 24 hours to establish a baseline potential.
- **Startup:** On the second day, the circuits were closed across a 25 Ω external resistor. Following a 48-hour stabilization period, continuous feeding of the anodic reactors was initiated at the designated flow rate to sustain steady-state power generation.

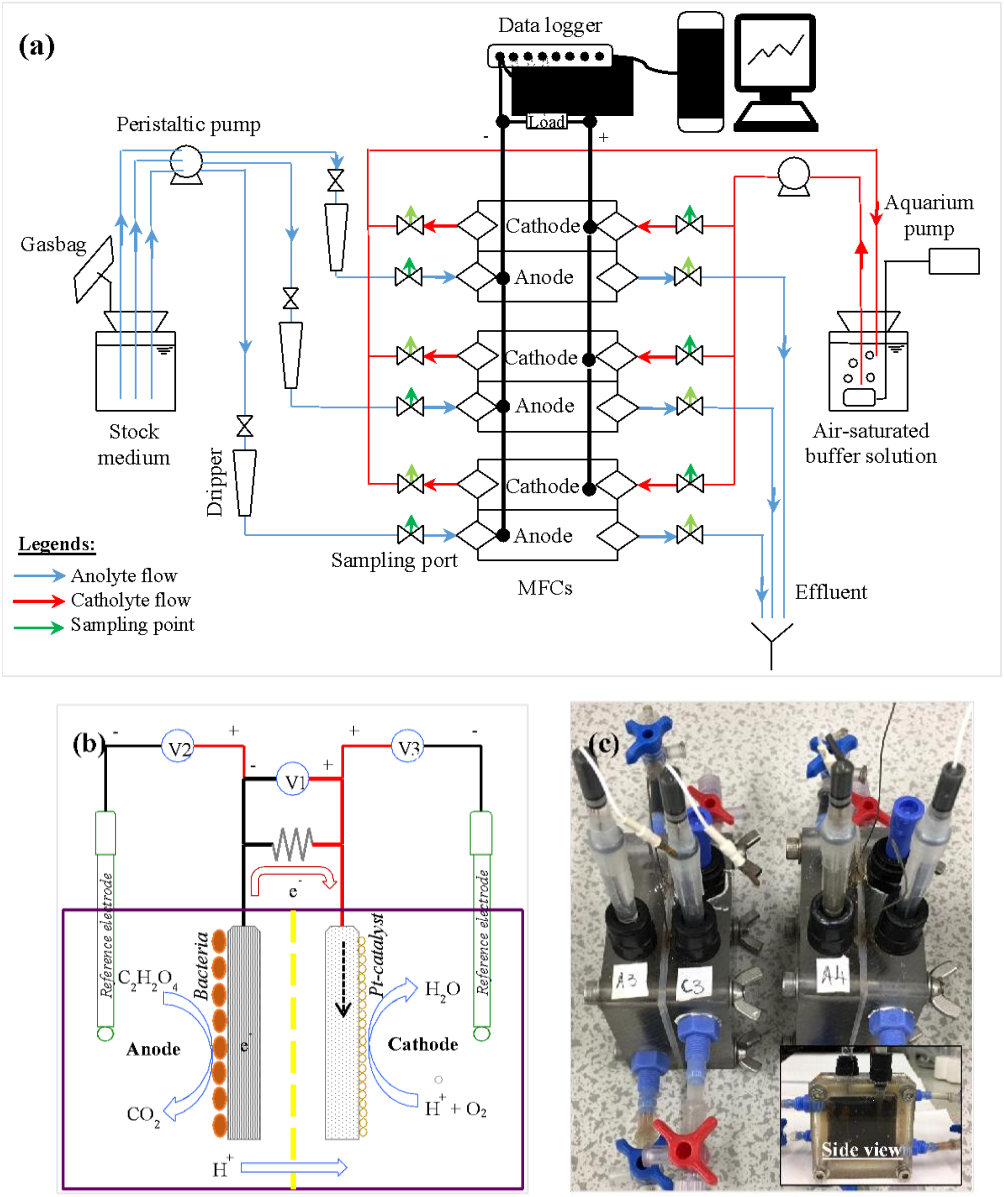

Figure 1 Schematic of (a) experiment arrangement, (b) single MFC and (c) the lab-scale MFCs

Electrochemical Characterization: EIS, CA, and CV

Upon reaching a steady-state power generation plateau (typically after >100 days of continuous operation), the MFCs were subjected to a suite of electrochemical analyses to characterize the internal resistance and kinetic behavior.

Electrochemical Impedance Spectroscopy (EIS)

Comprehensive impedance characterization was performed using a PGSTAT128N potentiostat equipped with an FRA32M frequency response analyzer module (Metrohm, Netherlands). To capture the full spectrum of electrochemical signatures—ranging from high-frequency ohmic shifts to low-frequency diffusion kinetics—measurements were conducted under Open Circuit Potential (OCP) across a frequency range of 100 kHz to 0.01 Hz, utilizing a resolution of 71 data points per logarithmic decade.

To achieve a high-resolution breakdown of the internal resistance (R_{int}), three distinct wiring configurations were employed:

- **Whole-Cell Analysis (2-Terminal):** Quantified the total internal resistance of the MFC, integrating all anodic, cathodic, and membrane-related losses.
- **Half-Cell Analysis (3-Terminal):** Utilized a reference electrode (SHE) to isolate the individual impedance of the bioanode and the abiotic cathode, focusing on the charge transfer resistance (R_1) and interfacial kinetics (R_2).
- **Membrane and Material Interface (4-Terminal):** Employed to measure the specific ohmic drop across the CMI-7000 membrane and the electrolyte, effectively separating bulk solution resistance (R_s) from the electrode-interface phenomena.

The resulting Nyquist and Bode plots were analyzed using Nova 11.1 software by fitting the raw data to a modified R(RQ)(RQT) equivalent circuit model. This approach allowed for the precise quantification of the capacitive element (T), the charge transfer resistance (R_1), and the interfacial resistance (R_2), providing a mechanistic map of the electrochemical bottlenecks within each cell component.

Stepwise Chronoamperometry (CA) and Polarization

To derive the polarization and power density curves, stepwise chronoamperometry was employed. The applied potential was decreased from the OCP to 0 V in decrements of 0.05 V. Each potential step was maintained for at least 15 minutes to ensure the system reached a pseudo-steady state. Only the stabilized current value at the end of each step was recorded for the construction of the polarization profiles.

Cyclic Voltammetry (CV)

Following the polarization tests, the MFCs were allowed to re-equilibrate under normal operating conditions for several days to ensure bioanode recovery. CV was then performed to evaluate the redox activity and electron transfer pathways of the biofilm.

- **Potential Range:** -0.5 V to +0.6 V vs. Standard Hydrogen Electrode (SHE).
- **Scan Rate:** 0.01 V/s (unless otherwise specified).
- **Data Selection:** At least three cycles were performed for each cell, with only the final scan used for analysis to ensure reproducibility.

Analytical Methods and Physicochemical Characterization

The organic strength and chemical environment of the MFCs were monitored using the following standardized protocols:

- **COD Analysis:** The organic concentration of the influent and effluent was quantified using high-range photometric cell test kits (Product No. 114541; range: 25–1500 mg/L) supplied by Merck, UK. Samples were prepared in reagent vials according to the manufacturer's procedures and determined colorimetrically using a Spectroquant® Pharo 300 spectrophotometer (Merck, UK).
- **pH and Conductivity Measurements:** The pH and electrical conductivity of the anolyte and catholyte were monitored using a calibrated multi-parameter meter to ensure a stable electrochemical environment.Anolyte Stability: The sodium acetate-based anodic medium was maintained at a near-neutral pH (7.0±0.2) to provide an optimal metabolic environment for the electrogenic microbial consortium.

- **Catholyte Conditions:** The 50 mM phosphate basal solution (pH 7.0) was monitored to ensure that proton consumption during the oxygen reduction reaction (ORR) did not result in localized pH shifts.
- **Correlation with Resistance:** Conductivity data was integrated with the EIS analysis to confirm that variations in solution resistance (R_s) were driven by physical connection quality rather than electrolyte fluctuations.

Mathematical Estimation and Mechanistic Correlation of Energy Losses

To quantify and interpret the overpotentials occurring during MFC operation, the polarization behavior was fitted using a semi-empirical model. This model dissects the cell potential (V) as a function of current density (I_D) by accounting for activation, ohmic, and mass-transport losses:

$$V = E_o - b\ log\ log\ I_D\ - RI_D - \gamma e^{\omega I_D} \qquad \textbf{(Equation 1)}$$

where V is the measured cell potential, E_0 is the theoretical open-circuit potential, b is the activation coefficient, R is the ohmic resistance coefficient, I_D is the current density, γ is the diffusion or concentration coefficient, and ω is the current consumption coefficient. The terms in Equation 1 were used to estimate the contribution of activation, ohmic, and concentration-related losses during MFC operation. The fitted parameters were then compared with the EIS and CV results to support the interpretation of the internal resistance effect.

The parameters are defined and correlated with physical characterization tools as follows:

- **V (V):** The final potential output, reflecting the cumulative energy losses in the system.
- **E_o (V):** The theoretical open-circuit potential where no energy loss occurs.
- **b (V) (Activation Coefficient):** Represents the initial potential energy required to activate redox reactions. This coefficient is directly linked to the charge transfer resistance (R_1) found in EIS and the midpoint potential shifts in CV. An increase in b (from 0.0266 V to 0.0415 V) correlates with the higher R_1 values in Groups 2 and 3, signaling a hindered initiation of electron transfer.
- **R (Ω) (Ohmic Coefficient):** Accounts for potential losses during electron and ion transport between electrodes. This parameter correlates with the solution resistance (R_s) and membrane resistance measured in EIS. The modeled R values (e.g., 3.18 Ω for Group 3) quantify the voltage drop caused by the physical poor connections or connection gaps identified in the experimental setup.
- **γ (V) and ω (m²/A) (Diffusion/Concentration Coefficients):** γ explains the energy consumed to transport reactants to the electrode surface, while ω estimates the rate of current consumption per surface area. These are validated by the Warburg element (W) in the EIS equivalent circuit and the linear relationship between peak current and scan rate in CV, which confirms whether the system is diffusion-limited.
- **Mechanistic Insight:** By linking these coefficients, the model suggests that increased internal resistance may not only increase ohmic loss, but may also contribute to activation and apparent mass-transport losses.

Results and discussion

Bioanode Enrichment and Steady-State Performance

The enrichment of electrogenic bioanodes was performed under continuous flow conditions (0.17 mL/min) to maintain a consistent substrate supply during the initial colonization phase.

Following this 50-day period, the operational mode was transitioned to fed-batch, which triggered a significant performance enhancement. As illustrated in Figure 2(a), the current density surged twofold, increasing from 0.15 to a stable plateau of 0.30 A/m^2. This trend aligns with typical microbial growth phases, where an initial logarithmic increase is followed by a steady-state maintenance period (Li et al., 2025; Lim et al., 2020).

The electron recovery was evaluated using Coulombic Efficiency (CE), which was calculated based on the total charge recovered from the current profile and the theoretical charge available from COD removal. The influent COD was approximately 363 mg/L, while the final COD values were 318, 292, and 305 mg/L for MFC Groups 1, 2, and 3, respectively. These values correspond to COD removals of approximately 45, 71, and 58 mg/L. Therefore, the CE result was interpreted together with the COD removal data to avoid overestimating electron recovery from the substrate.

Coulombic efficiency (CE) was calculated based on the ratio between the total charge recovered as current and the theoretical charge available from COD removal, as shown in Equation 2.

$$CE = \frac{M \int I\, dt}{FbV_{an}\Delta COD} \times 100 \qquad \textbf{(Equation 2)}$$

Where M is the molecular weight of oxygen (32 g/mol), I is the current (A), t is time (s), F is Faraday's constant (96,485 C/mol e^-), b is the number of electrons exchanged per mole of oxygen, V_{an} is the anode liquid volume (L), and ΔCOD is the COD removed during the operating period.

The shift to fed-batch operation was pivotal in this performance gain. This mode provides the electrogenic microbes with extended residence time, allowing for the comprehensive utilization of the organic content in the medium. The optimization of bioanode performance is intrinsically linked to the strategic management of operational modes and substrate availability. According to (Lim et al., 2017), providing a stable carbon source and appropriate applied potentials directly enhances microbial metabolism and catalytic activity within the biofilm. This is further supported by evidence that transitioning from continuous flow to fed-batch operation prevents the washout of essential metabolic intermediates, thereby yielding superior peak power densities and coulombic efficiencies. Ultimately, as identified in related studies on microbial electrolysis cells, the robust enrichment of the bioanode remains the primary determinant of total system performance, with mature biofilms capable of sustaining high oxidation rates (approximately 0.36 A/m^2) that mirror the steady-state results achieved in this study (Daud et al., 2018; Elreedy et al., 2024). This "recharge and utilize" cycle inherent in fed-batch operation allows the microbial consortium to maximize electron extraction per mole of substrate as substrate concentration remains constant throughout (Choudhury et al., 2020), thereby reducing mass-transport limitations that can occur in continuous systems with higher internal resistance (Rossi et al., 2021).

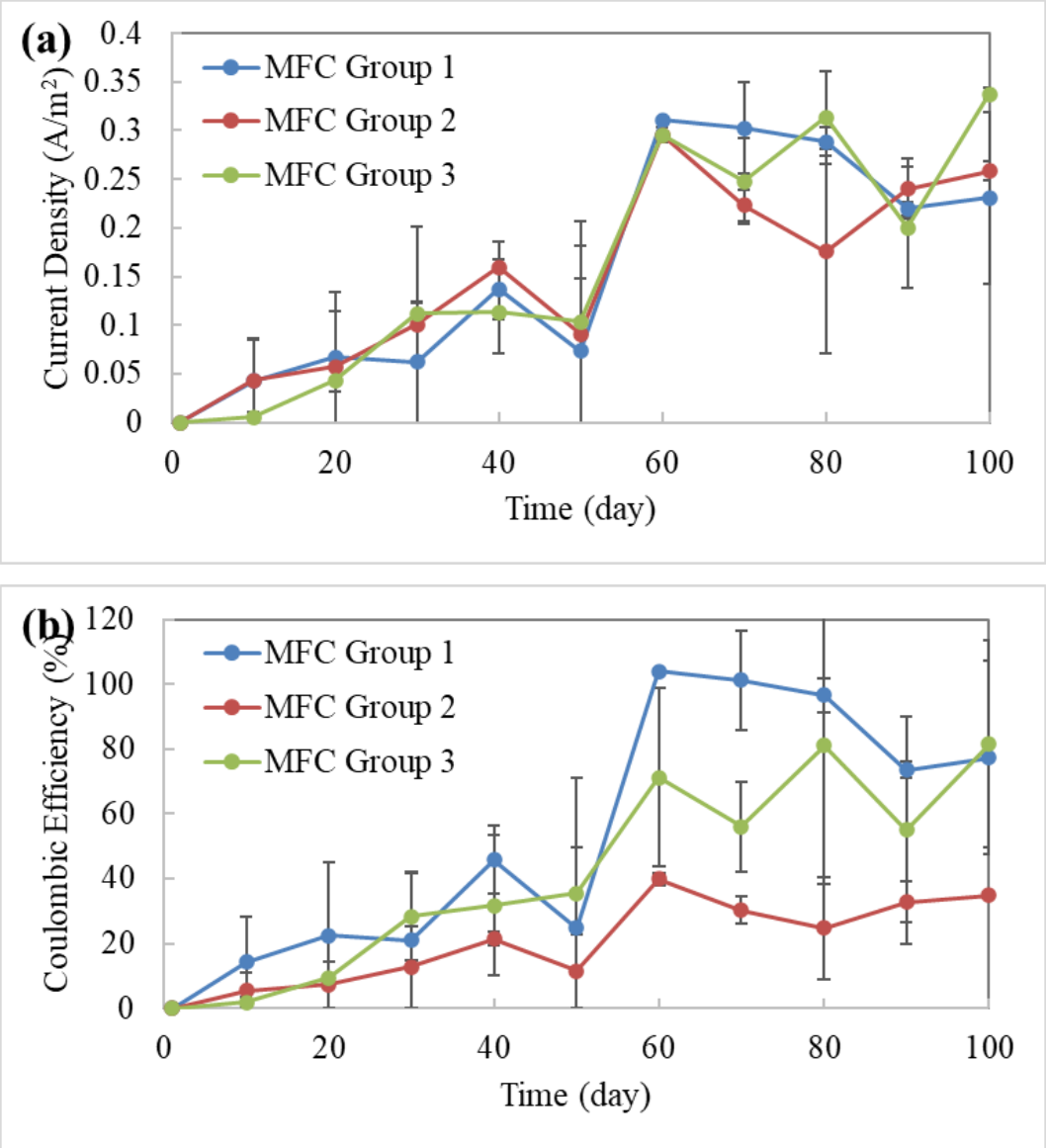

Figure 2 (a) Current density and (b) Coulombic efficiency of tested MFCs with different internal resistance. Data are presented as mean ± standard deviation from duplicate reactors (n = 2). Note that the current density plateaued after day 50.

Impact of Internal Resistance on Electrochemical Polarization

The internal resistance (R_{int}) serves as a critical bottleneck in the scalable power output of microbial fuel cells (MFCs). By deliberately manipulating the physical connectivity of the electrodes, we established a clear correlation between elevated R_{int} and the degradation of electrochemical performance (Chen et al., 2024). This relationship is quantitatively captured in Figure 3(a), where the polarization and power density curves reveal a systematic decline in maximum power output as the resistance gradation moves from Group 1 to Group 3.

The polarization behavior was modeled using Equation 1 to dissect the various energy losses (activation, ohmic, and concentration).

- **Maximum Power Density:** Group 1 achieved a peak power density of approximately 0.09 W/m^{2}at a current density of 0.22 A/m^2. In contrast, the significant connection restriction in

Group 3 limited the peak power to 0.07 W/m^2, representing a ≈ 22 % performance loss associated to the poor connection configuration.

- **Voltage Drop Trends:** As illustrated in Figure 3 (c), the voltage drop was most pronounced in Group 3 (black markers), where the increased ohmic coefficient (R) led to a steeper decline in cell potential compared to the optimized Group 1 (blue markers).
- **External Resistance Correlation:** The calculated external resistances at the peak power points were 414.0 Ω (Group 1), 476.5 Ω (Group 2), and 476.4 Ω (Group 3), indicating that the system's optimal load shifts slightly as internal losses increase.

To identify the specific physical origin of these losses, the charge transfer resistance (R_{ct}) was partitioned into cell components using Electrochemical Impedance Spectroscopy (EIS).

- **Anodic Bottleneck:** The bioanode was identified as the primary site of performance degradation. As seen in Figure 3 (d), the anodic resistance surged from a baseline of 3 ± 1 Ω in Group 1 to a staggering 135 ± 52 Ω in Group 3.
- **Total Cell Resistance:** The overall cell resistance followed the targeted experimental gradation, recording 16 ± 2 Ω for Group 1, 55 ± 8 Ω for Group 2, and 182 ± 6 Ω for Group 3. These values closely mirror the voltage-estimated resistance levels established in the methodology section (20, 60, and 180 Ω).

The data suggest that poor connection increased internal resistance, which then reduced MFC performance. This may be associated with changes in the apparent redox behavior caused by the increase in R_{int}. Recent literature indicates that when internal resistance is high, the biofilm may require higher electrochemical energy for electron transfer to overcome the anodic energy barrier (Ashiq et al., 2025; Miller et al., 2019). This shift is reflected in the positive midpoint potential transition observed in the CV results, moving from -0.2092 V (Group 1) to +0.1594 V (Group 3). This possible bioelectrochemical response may reduce the net potential difference for electricity generation, effectively widening the catalytic band and decreasing overall cell efficiency (Cao et al., 2012; Chadwick et al., 2019).

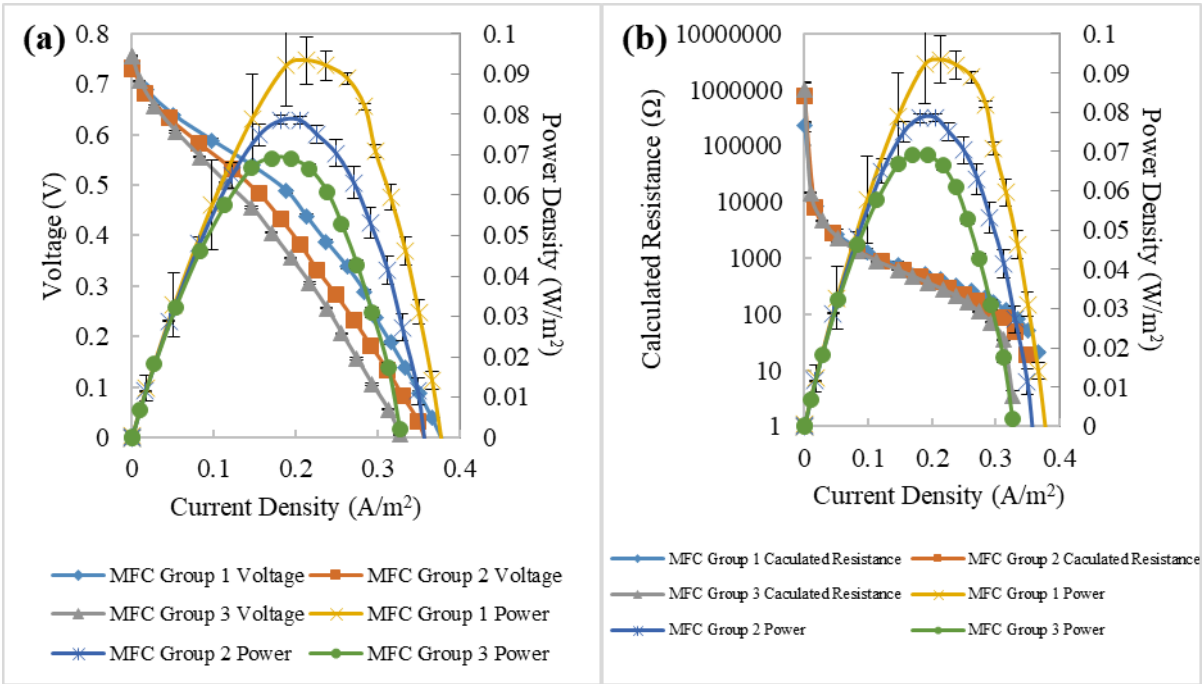

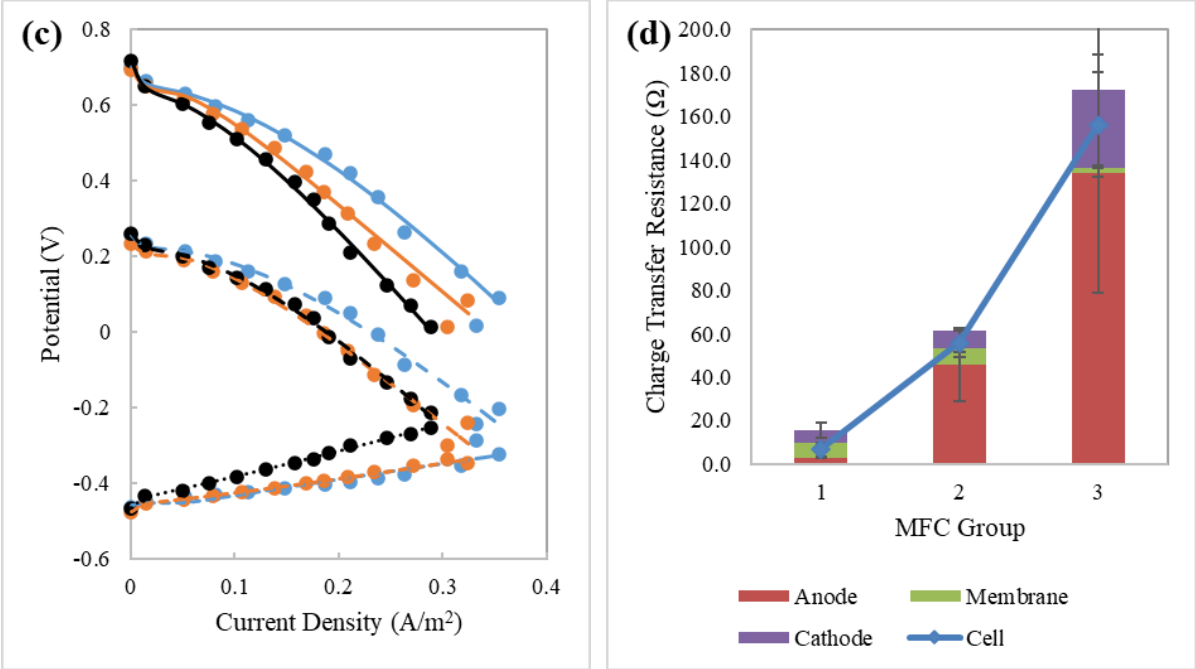

Figure 3 (a) Polarization and power curves, (b) calculated external resistance from a specific current withdrawn, (c) cell and half-cell potential and (d) charge transfer resistance of the MFC with different internal resistances. Data are presented as mean ± standard deviation from duplicate reactors (n = 2).

The empirical coefficients derived from the polarization equation (Table 2) confirm that internal resistance (R_{int}) does not act as an independent variable. Instead, it triggers a synergistic escalation across the three primary overpotential categories, fundamentally altering the cell's efficiency.

- **Ohmic Losses (R):** The ohmic coefficient reached its peak in Group 3 (3.1876 Ω for the cell; 3.4364 Ω for the summed components). This 13% increase relative to Group 1 (3.0875 Ω) is the direct mathematical manifestation of the poor connection design. The disparity between the measured "Cell" R and the "Sum" of components (R_{anode} + $R_{cathode}$) suggests that interfacial contact resistance at the titanium-carbon felt junction contributes significantly to the total voltage drop (iR drop).
- **Activation Losses (b):** A notable trend was observed in the activation coefficient, which rose from 0.0266V (Group 1) to 0.0415V (Group 3) This increase indicates that high R_{int} imposes a greater energy barrier for the initiation of electron transfer (López Zavala & Cámara Gutiérrez, 2023). Mechanistically, poor physical connectivity may require the electrogenic consortium to operate under higher electrochemical energy demand.
- **Mass Transport and Diffusion Losses (γ and ω):** The diffusion coefficient (γ) and the rate of current consumption (1/ω) showed significant variance across groups. In Group 3, the 1/ω value of -0.0988 A/m^2 suggests a more rapid onset of mass transport limitation compared to Group 1 (-0.2026 A/m^2). The fitted diffusion parameters suggest that the higher resistance condition was associated with greater concentration-related losses. However, because direct substrate concentration gradients of ion transport profiles were not measured, the result is interpreted as an apparent mass transport limitation rather than direct evidence of substrate diffusion limitation. This suggests that the higher-resistance condition may be associated with concentration-related losses at lower current densities

(Kanani et al., 2025), although direct ion transport or substrate gradient measurements would be required to confirm the specific mass-transport mechanism.

Table 2 Coefficients calculated from polarization equation (1) based on different internal resistance

Coefficient	Parameter	MFC Group 1	MFC Group 2	MFC Group 3
E_o (V)	Open Circuit Potential	1.2742	0.7623	0.9227
b (V)	Activation	0.0266	0.0372	0.0415
R (Ω)	Ohmic	3.0875	2.2496	3.1876
γ (V)	Diffusion	0.6682	0.2028	0.3553
1/ω (A/m^2)	Consumption Rate	-0.2026	-0.0496	-0.0988

Electrochemical Component Analysis and Resistance Distribution

The internal resistance (R_{int}) of the MFCs was partitioned using Electrochemical Impedance Spectroscopy (EIS) to identify the specific contributors to voltage de-rating. Theoretically, the total cell resistance is the summation of individual ohmic and non-ohmic components:

$$R_{cell} = R_{solution} + R_{anode} + R_{membrane} + R_{cathode} \quad \textbf{(Equation 3)}$$

To further elucidate the electrochemistry at the solid-liquid interfaces and within the bulk solution, each component represented in Equation 3 was decomposed into an equivalent electrical circuit (EEC). This approach allows for the characterization of electronic and ionic behaviors using resistors (R), constant phase elements (Q), and capacitive elements (T).

In this study, the EIS fitting parameters were used to identify the main source of resistance in the MFC. R_s represents the ohmic resistance from the electrolyte, membrane, and solution pathway. R_1 represents the charge transfer resistance, which is related to the electron transfer process at the electrode or biofilm–electrode interface. R_2 represents the interfacial resistance. In this study, R_2 may be related to the contact between the carbon felt and titanium wire, the porous structure of the carbon felt, and the interaction between the biofilm and electrode surface. The T element represents the pseudo-capacitive behavior of the porous biofilm/electrode interface, which is associated with charge storage and relaxation during the electrochemical process. Therefore, these parameters were used to explain how poor physical connection increased the resistance contribution in the MFC system.

As illustrated in Figure 4, distinct EEC models were employed to fit the high-resolution impedance data obtained from the 2-, 3-, and 4-terminal configurations:

- **Whole-Cell and Electrode Interface (Figure 4(a)):** The bioanode and cathode were modeled using an $R_s(R_1Q_1)(R_2Q_2T)$ configuration. Here, the nested RQ elements account for the porous nature of the carbon felt and the charge transfer resistance (R_1) at the biofilm-electrode interface. The inclusion of the T element specifically captures the pseudo-capacitive behavior of the electrogenic biofilm and the interfacial storage of ions (R_2).
- **Membrane and Solution Resistance (Figure 4(b)):** The membrane component was simplified to an $R_s(R_1Q_1)(R_2Q_2)$ circuit. This reflects the predominantly ohmic nature of the CMI-7000 separator (R_s) combined with the limited capacitive behavior (Q) arising from the ionic concentration gradient at the membrane-solution boundary.

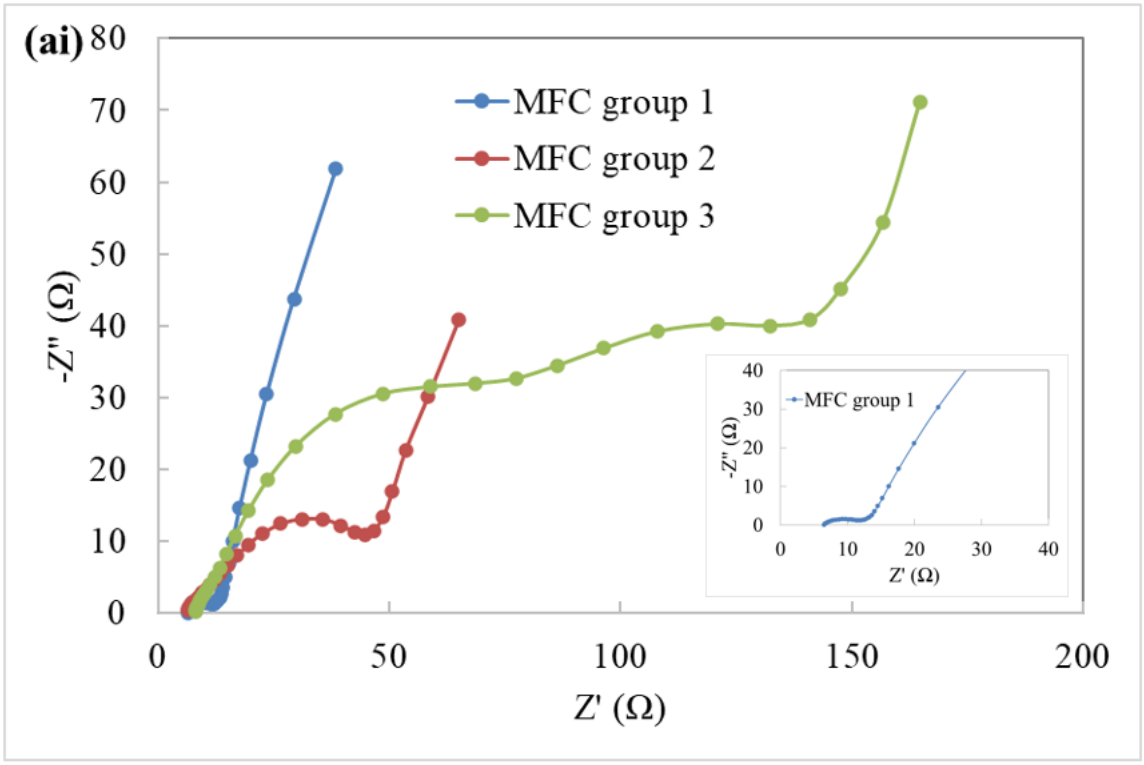
(ai)
MFC group 1
MFC group 2
MFC group 3
-Z'' (Ω)
Z' (Ω)
0
10
20
30
40
50
60
70
80
0
50
100
150
200
MFC group 1
-Z'' (Ω)
Z' (Ω)
0
10
20
30
40

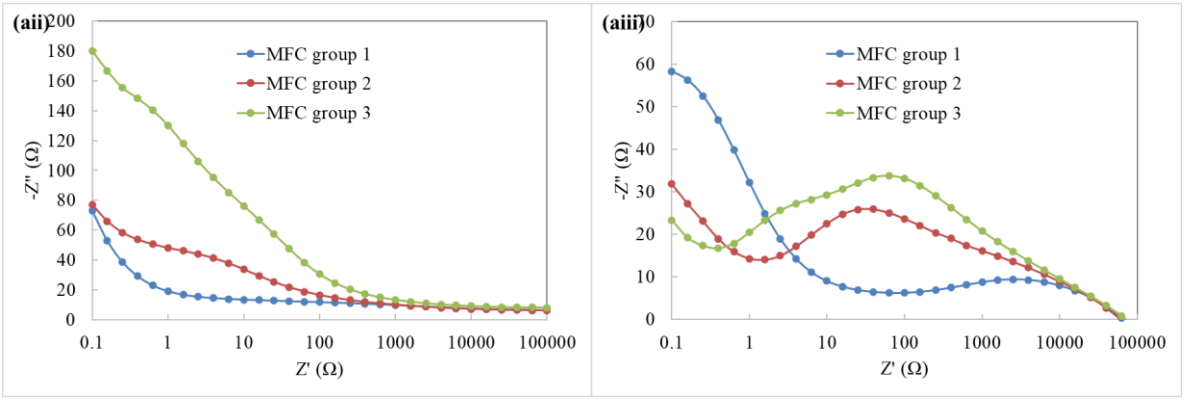
(aii)
MFC group 1
MFC group 2
MFC group 3
-Z'' (Ω)
Z' (Ω)
0.1
1
10
100
1000
10000
100000
(aiii)
MFC group 1
MFC group 2
MFC group 3
-Z'' (Ω)
Z' (Ω)
0.1
1
10
100
1000
10000
100000

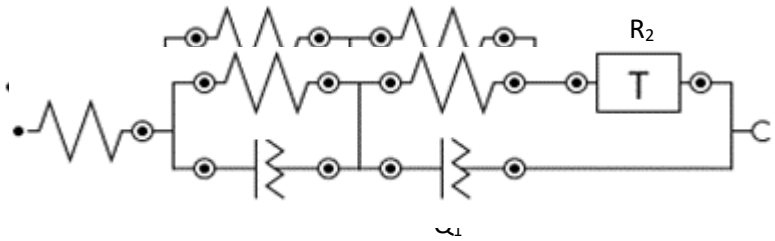
R2
T

(bii)

Figure 4 Electrochemical Impedance Spectroscopy (EIS) Characterization and Equivalent Electrical Circuit (EEC) Models. Sub-panels (a) illustrate the raw impedance spectra: (ai) Nyquist plots showing the distribution of ohmic and polarization arcs across MFC Groups 1–3; (aii) Bode magnitude plots depicting the frequency-dependent impedance response; and (aiii) Bode phase plots identifying the relaxation times of the bioelectrochemical interfaces. Sub-panels (b) present the fitted EEC configurations: (bi) The primary $R_s(R_1Q_1)(R_2Q_2T)$ model used to partition resistances in the whole cell, bioanode, and cathode, where T represents the pseudo-capacitive behavior of the biofilm; and (bii) The simplified $R_s(R_1Q_1)(R_2Q_2)$ model for the membrane component, isolating the ionic transport resistance from the electrode-interface kinetics. Solid lines in the spectra represent the best-fit data, with fit reliability confirmed by χ^2 values ≈ 0.005.

The breakdown of these resistances reveals that any increase in a specific component—most notably the Anode R_2 surge to 140.19 Ω in Group 3—directly correlates with the voltage drops observed in the polarization curves. Mechanistically, as R_{cell} increases, the system undergoes significant potential de-rating, which is manifested as a "widening" of the catalytic band in the CV derivatives. This widening signifies that a larger potential window is required to drive microbial electron transfer, effectively lowering the net power generation (Rosman et al., 2026).

By utilizing this multi-terminal EIS approach, the results suggest that the poor-connection condition in Group 3 mainly affected the anodic interfacial zone, transforming a highly conductive biofilm (0.6 Ω in Group 1) into the primary kinetic bottleneck of the entire system.

Table 3 Summary of fitted EIS internal resistance components for MFC Groups 1, 2, and 3. Values represent the mean ± fitting error from the data. Parameters were extracted using R(RQ)(RQT) equivalent circuit models.

Element	Parameter	MFC Group 1 (Value ± Error)	MFC Group 2 (Value ± Error)	MFC Group 3 (Value ± Error)
R_s (Ohmic)	R (Ω)	6.286 ± 0.787	5.874 ± 1.198	7.442 ± 0.386
R_1 (Charge Transfer)	R (Ω)	5.475 ± 0.763	17.597 ± 14.562	33.957 ± 22.773
Q_1 (CPE 1)	Y_0 (mS·s^n)	0.001 ± 0.000	0.002 ± 0.002	0.002 ± 0.002
	n	0.617 ± 0.057	0.651 ± 0.103	0.698 ± 0.257
R_2 (Interfacial)	R (Ω)	3.936 ± 3.601	31.515 ± 21.807	140.19 ± 28.800
Q_2 (CPE 2)	Y_0 (mS·s^n)	0.015 ± 0.002	0.006 ± 0.005	0.001 ± 0.000
	n	0.645 ± 0.064	0.512 ± 0.156	0.639 ± 0.100
T (Capacitive Element)	Y_0 (mS·s^n)	0.103 ± 0.077	0.133 ± 0.090	0.152 ± 0.117
	B	0.184 ± 0.155	0.184 ± 0.155	0.342 ± 0.238
χ^2 (Fit Quality)		0.005 ± 0.001	0.019 ± 0.005	0.005 ± 0.001

The data were fitted using the R(RQ)(RQT) equivalent circuit model, where the capacitive element (T) represents the biofilm's ability to store and transfer charge.

- **Capacitance (T) and Surface Roughness (B):** The Y_0 value of the T element increased from 0.103 (Group 1) to 0.152 mS·s^n (Group 3). This suggests that in high-resistance

environments, the biofilm may increase its thickness or surface complexity in a possible change in interfacial charge storage or biofilm/electrode response under high-resistance conditions (Vijay et al., 2023).

- **Fit Quality:** The low chi-squared (χ^2) values (≈ 0.005) across all groups confirm the high reliability of this model in describing the synergistic relationship between ohmic, kinetic, and interfacial energy losses.

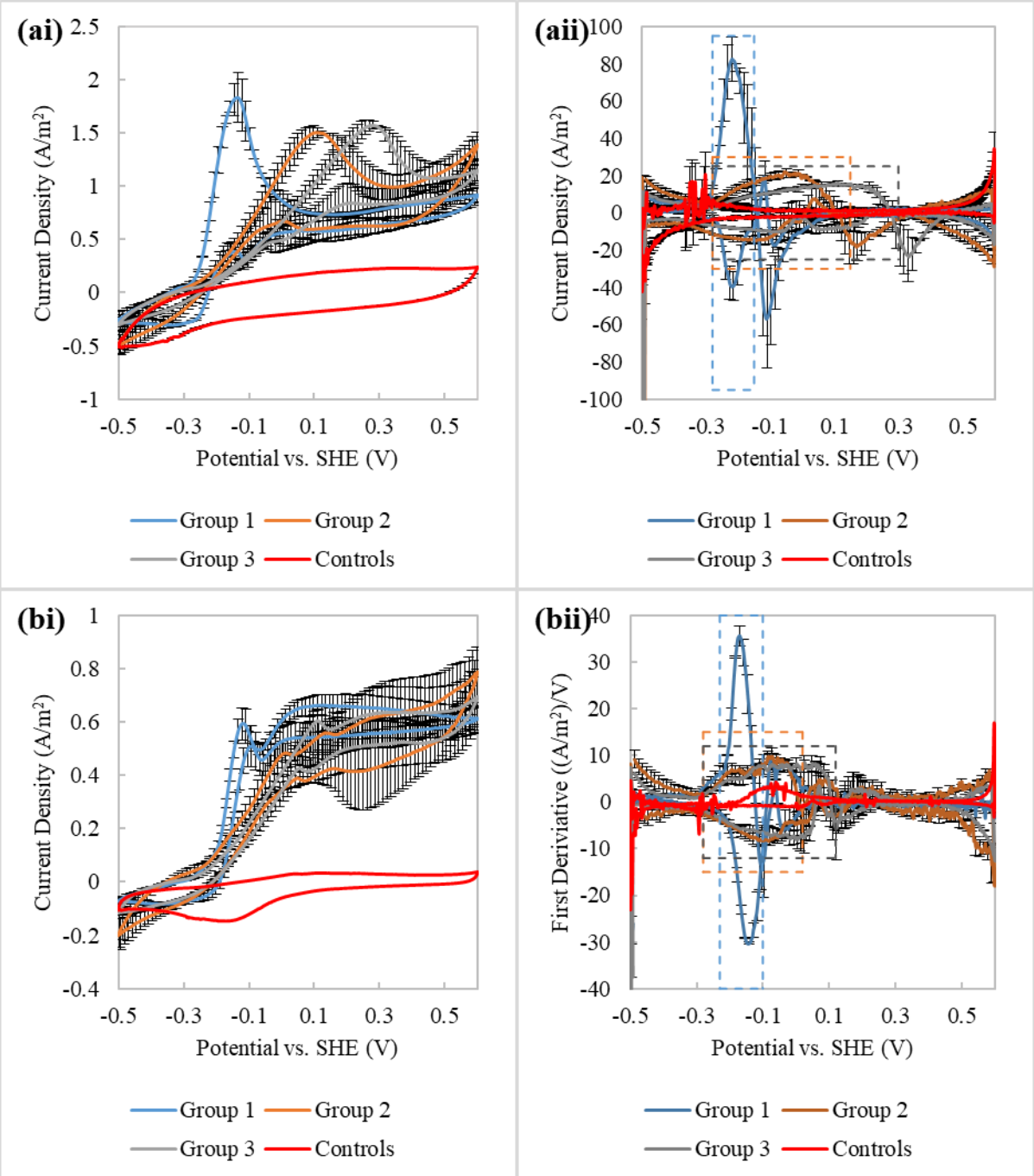

Figure 5 Bioelectrochemical characterization of enriched bioanodes via Cyclic Voltammetry (CV). Profiles were recorded at scan rates of (a) 0.01 V/s and (b) 0.001 V/s. Sub-panels illustrate: (i) the raw cyclic voltammograms highlighting

pseudo-reversible redox peaks, and (ii) the first-order derivative (dI/dV) of the forward scans used to pinpoint the midpoint potential (E_{mid}) and define the catalytic activity band. The widening of these bands across MFC Groups 1–3 suggests increased electrochemical energy demand and apparent overpotential development under higher internal resistance conditions.

Sensitivity Analysis: Effect of medium composition and ionic strength

This section is presented as a supporting sensitivity analysis and is separated from the main controlled internal resistance experiment. While the physical connection integrity remains the primary determinant of bioanode performance, the results in Figure 6 demonstrate that electrolyte composition significantly modulates the output by altering the solution resistance (R_s) and substrate availability. Using the OFAT approach, the impact of Sodium Acetate (NaAc), Ammonium Chloride (NH_4Cl), and Phosphate Buffer Solution (PBS) was evaluated against the baseline configuration (10:5:10 mM).

The most significant surge in current density, reaching a peak of ≈ 2.1 A/m^2 between days 59 and 61, was triggered by increasing the PBS concentration to 50 mM. This behavior is directly linked to a reduction in the internal resistance (Mohyudin et al., 2022) via two mechanisms:

- **Ohmic Reduction:** Higher PBS concentrations increase the ionic conductivity of the electrolyte, effectively lowering the R_s component of the total R_{int} (Guo et al., 2021).
- **Proton Transport:** Enhanced buffering capacity prevents localized pH drops within the bioanode biofilm, facilitating more efficient EET (Cao et al., 2022). Conversely, at low PBS concentrations (1 mM), the current density plummeted to < 0.2 A/m^2, suggesting that even with an optimized electrode connection, a poorly conductive medium can become the dominant limiting factor (Sydow et al., 2017).

The sensitivity to substrate concentration was less pronounced than that of the buffer. Increasing NaAc from 1 mM to 20 mM led to a gradual, incremental rise in current, plateauing around 0.5 A/m^2. This indicates that while the internal resistance dictates the "ceiling" of power output, substrate availability dictates the steady-state maintenance level. Similarly, the addition of NH^{4+} showed a minor positive correlation with performance, likely due to its role as a nitrogen source for biofilm maintenance and its minor contribution to the electrolyte's ionic strength (Ishaq et al., 2025).

These findings indicate that bioanode performance is a multi-variant function. To achieve maximum power density, it is important to address not only the poor physical connection (the physical R_{int}) but also optimize the "chemical R_{int}" (ionic strength). As seen in the sudden current drop when switching from 50 mM back to 10 mM PBS on day 61, a high internal resistance—whether caused by a loose titanium connector or a low-conductivity medium—may substantially reduce the catalytic activity of the biofilm (Gadkari et al., 2020; Guo et al., 2021).

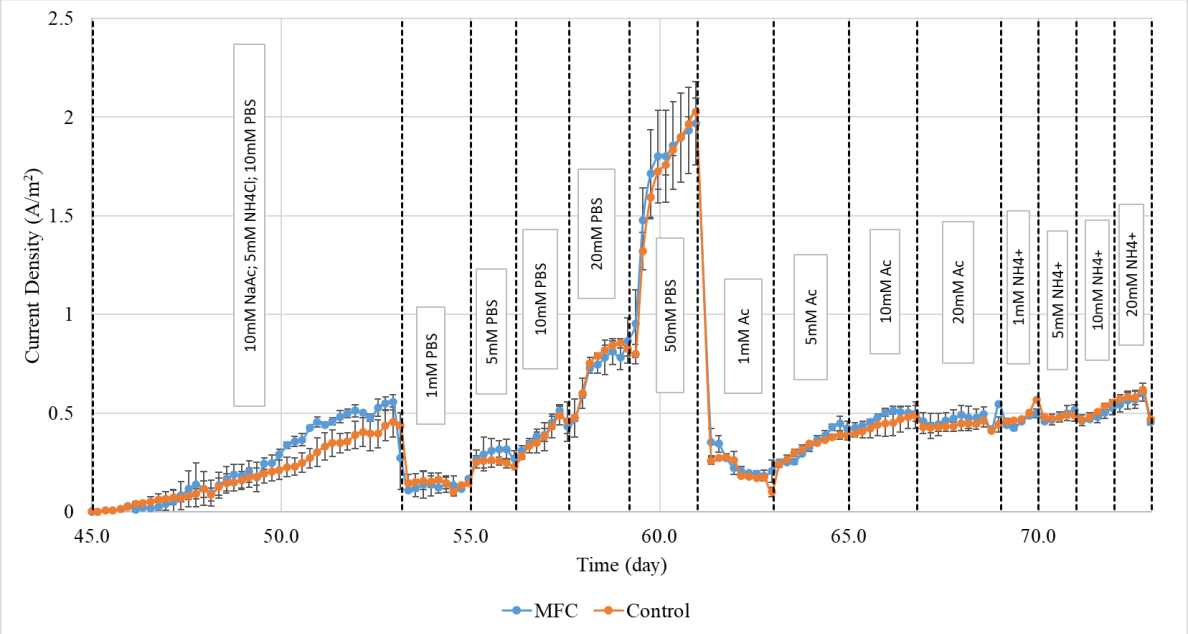

Figure 6 Dynamic Current Density Profile during OFAT Sensitivity Analysis. Continuous monitoring of bioanode current density during the systematic optimization of the anodic medium composition. The profile illustrates the transition from the baseline configuration (10:5:10 mM) to the optimized C:N:PBS ratio (10:5:50 mM). The marked surge to a peak of ≈ 2.1 A/m^2 on day 61 highlights the critical role of increased buffering capacity (50 mM PBS) in mitigating localized pH gradients and reducing solution resistance (R_s), thereby maximizing the electrocatalytic output of the enriched biofilm.

The OFAT sensitivity analysis identifies the 10:5:50 mM (NaAc:NH4Cl:PBS) ratio as the optimized medium composition for maximizing bioanode current density. While substrate and nutrient availability (NaAc and NH_4Cl) are essential for maintaining steady-state metabolic activity, the fivefold increase in buffer concentration (from 10 to 50 mM PBS) was shown to be the most influential chemical factor, driving the current density to a peak of ≈ 2.1 A/m^2. This suggests that in systems where physical internal resistance is already a challenge, maintaining high electrolyte conductivity and superior pH buffering is important to prevent a substantial decrease of the bioelectrochemical interface (Zhang et al., 2019).

Conclusion

This study quantified the effect of physical connection on internal resistance and bioanode performance in microbial fuel cells. By creating different resistance levels through controlled electrode–current collector contact conditions, the results showed that poor physical connection can increase internal resistance and reduce power output. This indicates that connection gaps, although often considered as minor assembly issues, can affect the stability and scalability of MFC performance.

The findings suggest that increased internal resistance does not only contribute to ohmic losses, but may also increase activation and diffusion-related losses. EIS analysis showed that the bioanode interface was the most affected component, with R2 becoming the main contributor to total cell resistance under poor-connection conditions. This highlights that the bioanode interface is highly sensitive to physical contact quality.

CV analysis showed a positive shift in apparent midpoint potential and broadening of the catalytic response at higher resistance. These changes suggest that the bioanode required higher electrochemical energy for electron transfer. However, this should be interpreted carefully because CV alone cannot confirm microbial metabolic adaptation or specific changes in electron-transfer pathways. Further biological analyses, such as microbial community analysis, biofilm imaging, EPS quantification, or mediator analysis, are needed to confirm whether these electrochemical changes are related to specific microbial or biofilm changes.

The OFAT analysis also showed that medium composition and ionic strength affected current generation, with 50 mM PBS improving buffering capacity and electrolyte conductivity. Overall, this study suggests that both physical connection and electrolyte composition should be considered when optimizing MFC performance.

Acknowledgements

The authors would like to express their gratitude to Universiti Kebangsaan Malaysia for supporting this research through the Research University Grant (GUP-2023-004) and Innovation Fund (INOVASI-2024-007). Financial support was also provided by the Malaysian Ministry of Higher Education under the Fundamental Research Grant Scheme (FRGS/1/2024/TK09/UKM/03/1) and the Pahang State Government via the Rompin State Park Forestry Research and Education Grant (RA-2024-003). Additionally, the authors gratefully acknowledge Mohd Asri Yusof, Mohd Fareeq Ahmad Fudzi, and Nik Samila Che Yusoff for their technical expertise and invaluable assistance with reactor fabrication, experimental design, and laboratory operations.

Author Contributions

Nor Syazwanie Mohd Saidi: Conceptualization, Methodology, Investigation, Data Curation, Writing – Original Draft. **Muhammad Farhan Hil Me:** Investigation, Validation, Visualization, Software (EIS Fitting). **Yashawini Phriya Rauichandran:** Investigation, Resources, Writing – Review & Editing. **Ryan Yow Zhong Yeo:** Investigation, Formal Analysis (CV Kinetics), Data Curation. **Mohammad Sherjeel Javed Khan:** Investigation, Validation, Writing – Review & Editing. **Swee Su Lim:** Conceptualization, Supervision, Project Administration, Funding Acquisition, Writing – Review & Editing.

Declaration of Competing Interest

The authors declare that they have no known competing financial interests or personal relationships that could have appeared to influence the work reported in this paper.)

References

Ashiq, N. M., Aldarmaki, A. A. J. A. R., Alketbi, M. S. S., Alshehhi, H. A. A., Alkaabi, A. S. O., Alshamsi, N. S. M. S., & Hassan, A. A. (2025). Challenges in Operating a Microbial Electrolysis Cell (MEC): Translating Biofilm Activity to Electron Flow and Hydrogen. *Sustainability*, *17*, 32. https://doi.org/https://doi.org/10.3390/su172411216

Baba, I. A., Abdulkareem, A. S., & Tijani, J. O. (2026). Photo-Fenton treatment of emerging pollutants in municipal wastewater using nanocatalysts: A sustainable approach. *Results in Chemistry*, *20*, 102999. https://doi.org/https://doi.org/10.1016/j.rechem.2025.102999

Boutarbouch, M., El-Moustaqim, K., Azoulay, K., Boudoudou, D., Abarkan, A., Moufti, A., & Mabrouki, J. (2026). Solar-Powered Electrochemical Processes for Sustainable Wastewater Treatment and Green Hydrogen Production: A Review [10.1051/bioconf/202621504009]. *BIO Web Conf.*, *215*.

Cao, B., Majors, P. D., Ahmed, B., Renslow, R. S., Silvia, C. P., Shi, L., Kjelleberg, S., Fredrickson, J. K., & Beyenal, H. (2012). Biofilm shows spatially stratified metabolic responses to contaminant exposure. *Environmental Microbiology*, *14*(11), 2901–2910. https://doi.org/https://doi.org/10.1111/j.1462-2920.2012.02850.x

Cao, M., Yin, J., Song, T., & Xie, J. (2022). Effects of the presence of phosphate buffer solution on removal efficiency of Pb and Zn in soil by solid phase microbial fuel cells. *Biotechnology Letter*, *44*, 11. https://doi.org/https://doi.org/10.1007/s10529-022-03315-1

Chadwick, G. L., Jiménez Otero, F., Gralnick, J. A., Bond, D. R., & Orphan, V. J. (2019). NanoSIMS imaging reveals metabolic stratification within current-producing biofilms. *Proceedings of the National Academy of Sciences*, *116*(41), 20716–20724. https://doi.org/10.1073/pnas.1912498116

Chen, T., Liu, H., & Li, J. (2024). Research on minimizing the MFC internal resistance via a shared electrode MFC-MEC coupling system [Article]. *Biochemical Engineering Journal*, *203*, Article 109195. https://doi.org/10.1016/j.bej.2023.109195

Choudhury, P., Ray, R. N., Bandyopadhyay, T. K., & Bhunia, B. (2020). Fed batch approach for stable generation of power from dairy wastewater using microbial fuel cell and its kinetic study. *Fuel*, *266*, 117073. https://doi.org/https://doi.org/10.1016/j.fuel.2020.117073

Daud, S. M., Daud, W. R. W., Kim, B. H., Somalu, M. R., Bakar, M. H. A., Muchtar, A., Jahim, J. M., Lim, S. S., & Chang, I. S. (2018). Comparison of performance and ionic concentration gradient of two-chamber microbial fuel cell using ceramic membrane (CM) and cation exchange membrane (CEM) as separators. *Electrochimica Acta*, *259*, 365–376. https://doi.org/https://doi.org/10.1016/j.electacta.2017.10.118

Elreedy, A., Härrer, D., Ali, R., Hille-Reichel, A., & Gescher, J. (2024). Efficacious enrichment of butyrate-oxidizing exoelectrogens upgrades energy recovery in relevant bioelectrochemical systems. *Environmental Technology & Innovation*, *36*, 103871. https://doi.org/https://doi.org/10.1016/j.eti.2024.103871

Environmental Requirements: A Guide For Investors (2010). Department of Environment Ministry of Natural Resources and Environment

Feng, F., Wu, C.-H., Li, F., Wang, X., Zhu, J., Zhang, R., & Chen, S.-C. (2024). Research on the integration of microbial fuel cells with conventional wastewater treatment technology: Advantages of anaerobic fermentation. *Energy Conversion and Management: X*, *23*, 100680. https://doi.org/https://doi.org/10.1016/j.ecmx.2024.100680

Gadkari, S., Fontmorin, J.-M., Yu, E., & Sadhukhan, J. (2020). Influence of temperature and other system parameters on microbial fuel cell performance: Numerical and experimental investigation. *Chemical Engineering Journal*, *388*, 124176. https://doi.org/https://doi.org/10.1016/j.cej.2020.124176

Guo, F., Luo, H., Shi, Z., Wu, Y., & Liu, H. (2021). Substrate salinity: A critical factor regulating the performance of microbial fuel cells, a review. *Science of The Total Environment*, *763*, 143021. https://doi.org/https://doi.org/10.1016/j.scitotenv.2020.143021

Hegazy, G. E., Soliman, N. A., Abdel-Fattah, Y. R., & Taha, T. H. (2025). Enhanced voltage generation in microbial fuel cells (MFCs) using bacterial isolates from seawater and industrial wastewater. *Microbial Cell Factories*, *25*(1), 21. https://doi.org/10.1186/s12934-025-02892-w

Ishaq, A., Said, M. I. M., Azman, S. B., Houmsi, M. R., Isah, A. S., Jagun, Z. T., Mohammad, S. J., Bello, A. A. D., & Abubakar, U. A. (2025). The influence of various chemical oxygen demands on microbial fuel cells performance using leachate as a substrate. *Environmental Science and Pollution Research*, *23*, 16.

Kanani, B., Zahedi, A., Abtahi, F., & Abedi, S. (2025). Exploring operational barriers in microbial fuel cells: Enhancing energy recovery from wastewater. *Electrochemistry Communications*, *180*, 108051. https://doi.org/https://doi.org/10.1016/j.elecom.2025.108051

Kim, B., Chang, I. S., Dinsdale, R. M., & Guwy, A. J. (2021). Accurate measurement of internal resistance in microbial fuel cells by improved scanning electrochemical impedance spectroscopy. *Electrochimica Acta*, *366*, 137388. https://doi.org/https://doi.org/10.1016/j.electacta.2020.137388

Kurniawan, S. B., Roziqin, A., Ahmad, A., Ahmad, M. M., Alfanda, B. D., Pambudi, D. S. A., Said, N. S. M., Abdul, P. M., & Imron, M. F. (2026). Tackling marine pollution in the blue economy: Synergies between wastewater treatment technologies and governmental policies. *Marine Pollution Bulletin*, *222*, 118627. https://doi.org/https://doi.org/10.1016/j.marpolbul.2025.118627

Li, Y., Zong, Y., Feng, C., & Zhao, K. (2025). The Role of Anode Potential in Electromicrobiology. *Microorganisms*, *13*, 23. https://doi.org/https://doi.org/10.3390/microorganisms13030631

Lim, S. S., Fontmorin, J.-M., Izadi, P., Wan Daud, W. R., Scott, K., & Yu, E. H. (2020). Impact of applied cell voltage on the performance of a microbial electrolysis cell fully catalysed by microorganisms. *International Journal of Hydrogen Energy*, *45*(4), 2557–2568. https://doi.org/https://doi.org/10.1016/j.ijhydene.2019.11.142

Lim, S. S., Fontmorin, J.-M., Pham, H. T., Milner, E., Abdul, P. M., Scott, K., Head, I., & Yu, E. H. (2021). Zinc removal and recovery from industrial wastewater with a microbial fuel cell: Experimental investigation and theoretical prediction. *Science of The Total Environment*, *776*, 145934. https://doi.org/https://doi.org/10.1016/j.scitotenv.2021.145934

Lim, S. S., Yu, E. H., Daud, W. R. W., Kim, B. H., & Scott, K. (2017). Bioanode as a limiting factor to biocathode performance in microbial electrolysis cells. *Bioresource Technology*, *238*, 313–324. https://doi.org/https://doi.org/10.1016/j.biortech.2017.03.127

López Zavala, M. Á., & Cámara Gutiérrez, I. C. (2023). Effects of External Resistance, New Electrode Material, and Catholyte Type on the Energy Generation and Performance of Dual-Chamber Microbial Fuel Cells. *Fermentation*, *9*(4), 344.

Mahmoud, R. H., Gomaa, O. M., & Hassan, R. Y. A. (2022). Bio-electrochemical frameworks governing microbial fuel cell performance: technical bottlenecks and proposed solutions [10.1039/D1RA08487A]. *RSC Advances*, *12*(10), 5749–5764. https://doi.org/10.1039/D1RA08487A

Miller, A., Singh, L., Wang, L., & Liu, H. (2019). Linking internal resistance with design and operation decisions in microbial electrolysis cells. *Environment International*, *126*, 611–618. https://doi.org/https://doi.org/10.1016/j.envint.2019.02.056

Mohyudin, S., Farooq, R., Jubeen, F., Rasheed, T., Fatima, M., & Sher, F. (2022). Microbial fuel cells a state-of-the-art technology for wastewater treatment and bioelectricity generation. *Environmental Research*, *204*, 112387. https://doi.org/https://doi.org/10.1016/j.envres.2021.112387

Musa, Y., Wee, B. S., Chung, H. H., Chin, S. F., & Lai, S. H. (2026). Microbial fuel cells as a sustainable nexus of wastewater treatment and bioelectricity generation: Advances, challenges, and future directions in a circular bioeconomy. *Renewable and Sustainable Energy Reviews*, *232*, 116799. https://doi.org/https://doi.org/10.1016/j.rser.2026.116799

Nawaz, A., Hafeez, A., Abbas, S. Z., Haq, I. u., Mukhtar, H., & Rafatullah, M. (2020). A state of the art review on electron transfer mechanisms, characteristics, applications and recent advancements in microbial fuel cells technology. *Green Chemistry Letters and Reviews*, *13*(4), 365–381. https://doi.org/10.1080/17518253.2020.1854871

Nemeș, N. S., Negrea, A., Ciopec, M., Negrea, P., Duţeanu, N., & Duda-Seiman, D. M. (2026). Heavy Metal Ion Removal: A Global Review of Wastewater Treatment Technologies. *International Journal of Molecular Sciences*, *27*(4), 1741.

Rani, M. N. A., Wahab, H. A., & Anuar, H. M. (2025). Toward Climate-Resilient Water Governance: A Legal and Policy Analysis of Malaysia's Water Sector. *International Journal of Environmental Sciences*, *11*.

Ravindran, V. H., Nuramidah, Mohd Arish, N. A., & Awang, M. (2025). Evaluation of Anaerobic and Aerobic Treatment for Tds, Cod, and

Bod Reduction in Meatball Wastewater *International Journal of Research and Innovation in Social Science*, *9*(5). https://doi.org/https://dx.doi.org/10.47772/IJRISS.2025.905000217

Rosman, N., Yusof, N., Norddin, M. N. A. M., Jaafar, J., Salleh, W. N. W., & Sa'adon, S. (2026). Performance evaluation of POME-based microbial fuel cells: treatment efficiency, power generation, and electron loss pathways. *Energy, Ecology and Environment*. https://doi.org/10.1007/s40974-026-00412-z

Rossi, R., Baek, G., Saikaly, P. E., & Logan, B. E. (2021). Continuous Flow Microbial Flow Cell with an Anion Exchange Membrane for Treating Low Conductivity and Poorly

Buffered Wastewater. *ACS Sustainable Chemistry & Engineering*, *9*(7), 2946–2954. https://doi.org/10.1021/acssuschemeng.0c09144

Saghir, M., Ayub, A., Nizami, A.-S., Baqar, M., Kamyab, H., Waqas, M., Rehan, M., & Asam, Z.-u.-Z. (2026). Sustainable valorization of leachate at Lakhodair landfill, Lahore: An integrated life cycle environmental and economic assessment of biogas production. *Biomass and Bioenergy*, *205*, 108540. https://doi.org/https://doi.org/10.1016/j.biombioe.2025.108540

Solomon, D., Kiflie, Z., & Van, H. S. (2020). Integration of sequencing batch reactor and homo - catalytic advanced oxidation processes for the treatment of textile wastewater. *Nanotechnol Environ Eng*, *6*. https://doi.org/10.1007/s41204-020-0070-6

Sydow, A., Krieg, T., Ulber, R., & Holtmann, D. (2017). Growth medium and electrolyte—How to combine the different requirements on the reaction solution in bioelectrochemical systems using Cupriavidus necator. *Engineering in Life Sciences*, *17*(7), 781–791. https://doi.org/https://doi.org/10.1002/elsc.201600252

Vijay, A., Ghosh, P. C., & Mukherji, S. (2023). Power Generation by Halophilic Bacteria and Assessment of the Effect of Salinity on Performance of a Denitrifying Microbial Fuel Cell. *Energies*, *16*(2), 877.

Wang, A., Klassert, C. J. A., Karutz, R., Smilovic, M., Kahil, T., Burek, P., Zhu, Y., Zozmann, H., Klauer, B., Küblböck, K., Omann, I., Figueroa, A. J., Wada, Y., Naylor, R., & Gorelick, S. M. (2026). Drought-Driven Water Insecurity in an Emerging Indian Megacity: A Coupled Multi-Agent Systems Approach for Policy Evaluation. *Earth's Future*, *14*(3), e2025EF007976. https://doi.org/https://doi.org/10.1029/2025EF007976

Wilk, B. K., Szopińska, M., Sobaszek, M., Pierpaoli, M., Błaszczyk, A., Luczkiewicz, A., & Fudala-Ksiazek, S. (2022). Electrochemical oxidation of landfill leachate using boron-doped diamond anodes: pollution degradation rate, energy efficiency and toxicity assessment. *Environmental Science and Pollution Research*, *29*, 17.

Zadeh, P. G., Rezania, S., Fattahi, M., Dang, P., Vasseghian, Y., & Aminabhavi, T. M. (2024). Recent advances in microbial fuel cell technology for energy generation from wastewater sources. *Process Safety and Environmental Protection*, *189*, 425–439. https://doi.org/https://doi.org/10.1016/j.psep.2024.06.077

Zhang, X., Li, X., Zhaoa, X., & Li, Y. (2019). Factors affecting the efficiency of a bioelectrochemical system: a review. *RSC Advances*, *9*, 14.